Small-angle x-ray scattering measurements of the microstructure of liquid helium mixtures adsorbed in aerogel

L. B. Lurio

Department of Physics, Northern Illinois University, DeKalb, Illinois 60115, USA

N. Mulders

Department of Physics, University of Delaware, Newark, Delaware 19716, USA

M. Paetkau

Department of Physics and Astronomy, Okanagan College, British Columbia V1Y4X8, Canada

M. H. W. Chan

Department of Physics, Pennsylvania State University, University Park, Pennsylvania 16802, USA

S. G. J. Mochrie

Department of Physics, Yale University, New Haven, Connecticut 06511, USA

Small-angle x-ray scattering (SAXS) was used to measure the microstructure of isotopic mixtures of ^{3}He and ^{4}He adsorbed into silica aerogels as a function of temperature and ^{3}He concentration. The SAXS measurements could be well described by the formation of a nearly pure film of ^{4}He which separates from the bulk mixture onto the aerogel strands and which thickens with decreasing temperature. Previous observations of a superfluid ^{3}He-rich phase are consistent with superfluidity existing within this film phase. Observed differences between different density aerogels are explained in terms of the depletion of ^{4}He from the bulk mixture due to film formation.

I. INTRODUCTION

Silica aerogels consist of a dilute network of SiO_2 strands connected at random sites. They can be extremely porous, having an open volume of up to 99.5%, and because of this, they have frequently been used as model systems to study the effects of weak perturbations on liquids [1,2]. The effect of confinement in aerogel on the phase diagram of liquid helium mixtures is particularly striking. In bulk mixtures of liquid ^{3}He and ^{4}He the superfluid transition temperature decreases with increasing ^{3}He concentration until it reaches a tricritical point. At temperatures below this tricritical point helium mixtures phase separate into a superfluid ^{4}He-rich component and a normal fluid ^{3}He-rich component. In the limit of the temperature approaching zero, the ^{3}He-rich fluid completely excludes ^{4}He, while on the ^{4}He-rich side of the coexistence curve 6.4% ^{3}He remains in the mixture at $T=0$. Kim, Ma, and Chan [3] first observed the phase diagram of helium mixtures in 98% open volume aerogel using a torsional oscillator. They found that inside aerogel the tricritical point disappears and the λ line separates from the phase-separation line. Thus, for fixed temperature, as the ^{3}He concentration X_3 increases, there is a region of ^{4}He-rich superfluid phase, a region in which the mixture phase separates, a region of ^{3}He-rich superfluid, and a region normal-fluid ^{3}He-rich phase (see Fig. 8). Furthermore, they found that even in the limit of $T=0$ approximately 4% ^{4}He remains in the ^{3}He-rich phase.

The most likely cause for the strong influence of aerogel on the phase diagram of helium mixtures is that aerogel preferentially attracts ^{4}He since the density of liquid ^{4}He is around 25% larger than the density of ^{3}He. One can imagine two possible explanations for the unusual observation of a ^{3}He-rich superfluid phase in aerogel. One possibility is that ^{4}He forms a superfluid film on the aerogel which is then immersed in a normal ^{3}He-rich mixture. The other possibility is that there is a mixed ^{3}He-rich superfluid with possibly some preference for ^{4}He within the mixture to be closer to the aerogel. Kim, Ma, and Chan argued for the second alternative based on the observation that the properties of a superfluid ^{4}He film in the absence of a ^{3}He-rich mixture were quite different than the properties of the ^{3}He-rich superfluid. For example, a superfluid film would be expected to show a linear dependence of T_c on ^{4}He coverage, which was not seen in the mixtures.

The experimental observations of Kim, Ma, and Chan were later supported by theoretical calculations of Falicov and Berker [4]. They observed that the effect of aerogel on helium was similar to that of a random bond interaction. Furthermore, a random bond interaction was expected on theoretical grounds [5,6] to convert a first-order phase transition which involves symmetry breaking into a second-order transition. In the present instance, the first-order transition is the phase separation between the ^{3}He-rich and ^{4}He-rich phases, and the symmetry is the superfluid order parameter. Thus this theory predicts that the superfluid transition should separate from the helium demixing line as seen by Kim, Ma, and Chan. Falicov and Berker also performed a Monte Carlo simulation in the context of a Blume-Emery-Griffiths model [7]. This yielded a phase diagram in remarkable agreement

with the diagram observed by Kim, Ma, and Chan. The theoretical phase diagram showed both the separation of the λ line from the demixing line and a finite concentration of ^{4}He in the ^{3}He-rich component at $T=0$. Similar theoretical results were also found by Maritan *et al.* [8].

Further experimental studies of the phase diagram were performed by Mulders and Chan [9]. They used heat capacity as a probe of the phase transitions and found a phase diagram essentially identical to the one found by Kim, Ma, and Chan. Furthermore, they found that there was a peak in the heat capacity across the λ line in the ^{3}He-rich part of the phase diagram. Since a heat capacity peak is not observed for pure ^{4}He films [10], they conclude that its existence indicates a bulklike phase for the ^{4}He in the ^{3}He-rich component. They suggest, however, a modification of the ideas of Kim, Ma, and Chan. Rather than a superfluid mixed phase, superfluidity occurs within a broad interfacial region between the ^{4}He film and the ^{3}He-rich phase.

Somewhat different behavior was observed by Paetkau and Beamish [11] who used ultrasound to study the properties of helium mixtures in an 87% open volume aerogel. As with the earlier studies, they found a second-order transition in the ^{3}He-rich portion of the phase diagram and a ^{3}He-rich superfluid phase for $X_3 < 0.8$. However, on the ^{3}He-rich side of the phase diagram, they did not see any specific signature of phase separation.

Later work by Tulimieri, Yoon, and Chan [12] found that 70% porous gold showed a phase diagram nearly identical to that of 98% open volume aerogel. Based on a comparison with ^{4}He adsorption isotherm data they argued that the ^{3}He-rich superfluid phase consisted of superfluidity along a thick ^{4}He film.

All of these earlier studies have found that the phase behavior of helium mixtures is significantly modified in aerogel, with the first-order demixing transition replaced by a second-order superfluid transition. In lighter aerogels, there appears to be a second separate demixing transition, not observed in 87% open volume gels. In all cases, the ^{3}He-rich phase does not completely exclude the ^{4}He fraction at $T=0$. What has been left an open question is the microscopic nature of the inhomogeneous mixture at large X_3. Does superfluidity occur within a mixed (if not completely isotropic) ^{3}He-rich phase or does superfluidity occur within a thickened film phase? The inability of these measurements to answer this question is, in some sense, not surprising, since torsional oscillators, heat capacity, and ultrasound all probe samples at macroscopic length scales. In order to definitively answer the question of the microstructure of the helium phases it is necessary to use a probe which has resolution at the length scale of the aerogel microstructure ($\sim 1-100$ nm). For this reason, we have chosen to use small-angle x-ray scattering (SAXS) to study the microstructure of helium mixtures.

It might appear, at first glance, that neutrons would be a preferable choice to x rays for such studies, since neutrons can resolve the two different isotopes of helium, while x rays cannot. However, the large inelastic neutron-scattering cross section of ^{3}He makes such studies difficult. At the same time, the large density difference (25%) between liquid ^{3}He and ^{4}He provides more than sufficient contrast to perform x-ray-scattering measurements.
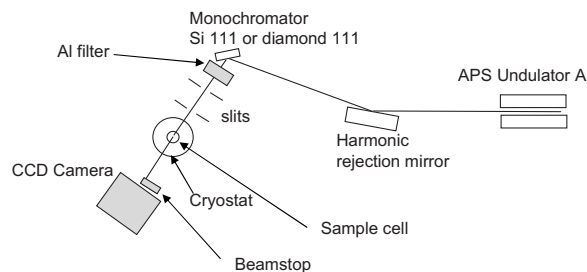
FIG. 1. Schematic of experimental setup at the Advance Photon Source Sector 8.

II. EXPERIMENT

Aerogels were grown by base-catalyzed polymerization of silica which was then supercritcally dried. This procedure produced a multiply connected random silica network possessing distinct structures over a range of length scales from 1 to 100 nm. Aerogels with open volume fractions of 98% and 87% were produced. The aerogels were grown as cylindrical disks and then placed into close-fitting open copper cylinders of thickness 4.3 mm and 3.3 mm, respectively. These were then sealed between two 1.33-in. SS conflat flanges equipped with beryllium end windows. The sample cells were cooled within a closed-cycle cryostat which employed a PT405 pulse-tube refrigerator and a pumped liquid ^{3}He pot. The base temperature of the cryostat was around 450 mK. Helium films and helium mixtures were dosed through a thin capillary tube in the side of the sample chamber which communicated with a gas-handling system held outside the cryostat.

The cryostat was mounted on a spectrometer at the 8-ID station of the Advanced Photon Source (APS) at Argonne National Laboratory. The cryostat was precooled with the sample inside and then mounted while cold onto the spectrometer. Since an area detector was used to measure the SAXS, no motion of the cryostat was necessary during the experiment other than the initial alignment of the windows. The scattering setup is shown in Fig. 1. Measurements were made at an x-ray energy 22.4 keV generated from the third harmonic of an APS undulator A as well as at 7.45 keV using first harmonic of the undulator. When making measurements at the third harmonic an aluminum filter was used to remove the first harmonic. For the first-harmonic measurements the higher-energy harmonic was removed using a mirror. Either a Si-111 or a diamond-111 monochromator crystal was used to define the energy of the beam. A set of slits was used to define a beam size of 100 mm $\times$ 100 mm and a second set of downstream slits was used to trim slit scatter. The sample scattering was measured using a charge-coupled-device (CCD) camera coupled to a phosphor screen via a 2.4-1 optical capillary taper. Data were corrected for flat-field and distortion errors introduced by the phosphor and capillary taper. The intensity of x rays transmitted through the cryostat was measured using a p-i-n diode mounted on a beamstop in front of the camera. The small-angle scattering data were placed on an absolutely calibrated intensity scale by reference to a previously calibrated standard.
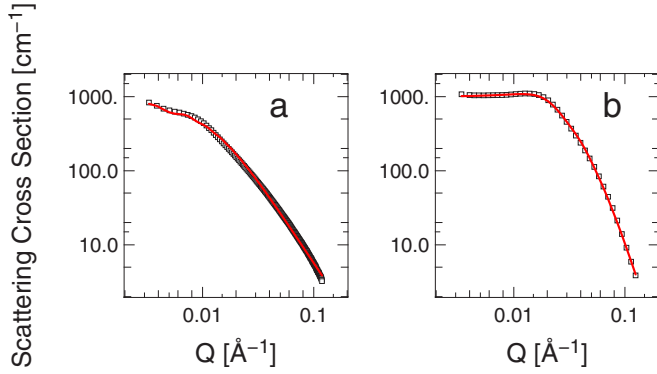
FIG. 2. (Color online) Scattering cross section from 98% porous (a) and 87% porous (b) aerogels. Solid lines are fits to measured data using the model described in the text.

III. X-RAY SCATTERING FROM BARE AEROGELS

Measurements were first made on the empty aerogels in order to characterize their structure. The SAXS cross sections from 98% and 87% porosity aerogels are shown in Fig. 2. These measurements were fit to the simulated scattering obtained from a parametrized model of the aerogel structure using a nonlinear least-squares fitting algorithm. The aerogel was modeled as a fractal network [13] of small spheres of radius r with a correlation length ξ. At length scales $R > \xi$ different fractal clusters were assumed to interact and pack together. The x-ray scattering from such a model is the product of three structure factor terms, one corresponding the form factor of the individual silica spheres, $S_s(Q)$; one corresponding to the form factor of the fractal clusters, $S_f(Q)$; and one corresponding to cluster-cluster correlations, $S_c(Q)$. Mathematical expressions for these structure factors have been given by Posselt *et al.* [14] based on the fractal form factor derived by Freltoft *et al.* [13]. This structure factor (per electron) can be normalized and placed on an absolute scale as described by Teixeira [15]. Thus we take as a properly normalized structure factor model for aerogel the following:

$$S(Q) = S_c(Q)S_f(Q)S_s(Q), \qquad (1)$$

$$S_c(Q) = \frac{1}{1 + 8\rho\Theta(QR)}, \qquad (2)$$

$$S_f(Q) = 1 + \frac{1}{(QR)^{d_f}} \frac{d_f\Gamma(d_f - 1)\sin(d_f - 1)\tan^{-1}(Q\xi)}{[1 + 1/(Q\xi)^2]^{(d_f-1)/2}}, \qquad (3)$$

$$S_s(Q) = \left[1 + \frac{2}{9}(Qr)^4\right]^{-1}. \qquad (4)$$

Here the scattering vector $Q = 4\pi \sin(\theta/2)/\lambda$ with θ the scattering angle of the x-ray beam and λ the x-ray wavelength. The parameter ρ characterizes the interactions between nearby fractal clusters and can be viewed as a packing fraction. The function $\Theta(QR) = 3[\sin(QR) - QR\cos(QR)]/(QR)^3$ is the form factor of a sphere. The data could be fit reasonably well using this model as shown by the solid lines. Be-

TABLE I. Results of fits to bare aerogel scattering.

	r (Å)	d_f	ξ (Å)	R (Å)	ρ
98% Aerogel	6.2±0.1	2.18±0.03	94±4	609±68	0.32±0.12
87% Aerogel	5.2±0.2	3.1±0.1	31±2	275±10	0.69±0.07

low $Q < 0.005$ there is a small contribution from parasitic scattering from the beryllium windows. The best-fit parameters obtained from the fits are given in Table I. As expected the denser gel has a higher fractal dimension, a smaller cluster size, and a higher packing fraction. Better simulations of the structure from aerogels can be achieved using numerical simulations as was done by Hasmy *et al.* [16], but it would be nontrivial to adjust such models so as to give the best fit to the measured data.

IV. ⁴He FILMS ON AEROGEL

Small-angle x-ray scattering measurements were then made on pure ⁴He films which were grown by dosing gas into the sample chamber containing aerogel at low temperature ($T = 0.50$–0.60 K). Scattering patterns are shown in Fig. 3 for varying helium filling fractions f_4. The filling fractions are defined as the ratio of the number of moles of ⁴He admitted into the sample chamber divided by the number of moles required to fill the chamber with liquid ⁴He. For clarity, not all data sets are shown in the figure. Qualitatively, the scattering intensity is seen to increase at small Q as the filling fraction is increased, but then between 20% and 24% filling fraction the intensity at small Q disappears and the scattering curve collapses back to nearly its original value.

In order to understand the behavior quantitatively, it is necessary to construct a model for the scattering. We con-
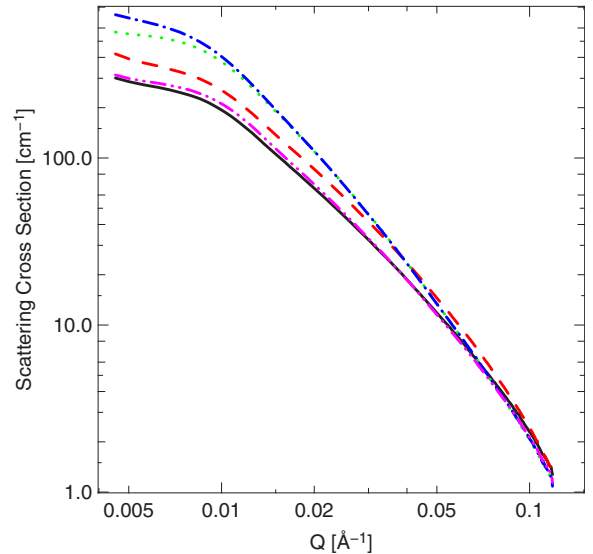
FIG. 3. (Color online) Scattering from aerogel as a function of ⁴He filling fraction f_4 over the range $T = 0.45$–0.60 K. Solid line (black), empty aerogel; dashed line (red), $f_4 = 4\%$; dotted line (green), $f_4 = 16\%$; dash-dotted line (blue), $f_4 = 20\%$; dash-double-dotted line (magenta), $f_4 = 24\%$.

sider the individual contributions to the scattering from helium and silica by writing the electron density as the sum $\rho_e = \rho_{SiO_2} + \rho_{He}$ and assume that the helium density variations are correlated with the aerogel density up to a crossover length L. A similar model was used to describe the correlations between a binary fluid and an aerogel by Frisken *et al.* [17]. This model yields a functional form for the ratio of the measured scattering to the scattering from the empty aerogel given by

$$\frac{I(Q)}{I_e(Q)} \approx \frac{C_1^2 + C_2^2 Q^2 L^2}{1 + Q^2 L^2}, \tag{5}$$

$$C_1 = \frac{f_{SiO_2}\rho_{SiO_2} + f_4\rho_4}{f_{SiO_2}\rho_{SiO_2}}, \tag{6}$$

$$C_2 = \frac{\rho_{SiO_2} - \rho_4}{\rho_{SiO_2}}. \tag{7}$$

Here f_{SiO_2} is the volume fraction occupied by the silica and f_4 the volume fraction occupied by the helium film. If the helium, due to surface tension, collapses into clusters whose size or shape is not correlated with the structure of the aerogel, then this would produce additional scattering which is not accounted for in this model.

In addition, one might also expect an oscillation in the scattering intensity at large Q due to interference between the scattering from the top and bottom interfaces of the helium film. Such an oscillation was searched for, but not found. We hypothesize that this may be due to the surface of the aerogel not being well defined but rather consisting of a loose network of strands. Thus, there may not be a sufficiently well-defined film thickness to result in interference oscillations.

As indicated in Eq. (5) it is useful to plot the data in the form $R(Q) = I(Q)/I_e(Q)$. This is shown in Fig. 4. The symbols represent the experimental data, while the solid lines are fits to the data using Eqs. (5)–(7). In the fits to the data, two parameters were varied: the crossover length L and the filling fraction f_4. The resulting values of the best-fit parameters are plotted in Figs. 5(a) and 5(b). The model describes the shape of the data well. The increase in the scattering intensity at small Q correlates very well with the filling fraction as seen in Fig. 5(b). However, for filling fractions between 16% and 24% the scattering intensity no longer increases, but instead collapses back to nearly its original value. The exact filling fraction where the collapse occurs shows histeresis, as would be expected for capillary condensation. When the cell is completely filled with liquid ^{4}He the scattering intensity is nearly identical to that of the empty cell, except for a reduction in intensity due to the reduced contrast of silica-^{4}He compared with silica-vacuum.

The best fit crossover length increases monotonically with increasing fill fraction, indicating that as more ^{4}He liquid is admitted to the cell, larger and larger structures within the aerogel are filled. At very small filling fractions the pore size appears to flatten out. This is most likely due to the difficulty in resolving small length scales due to the limited Q range of the data. The best-fit crossover length also shows, over a
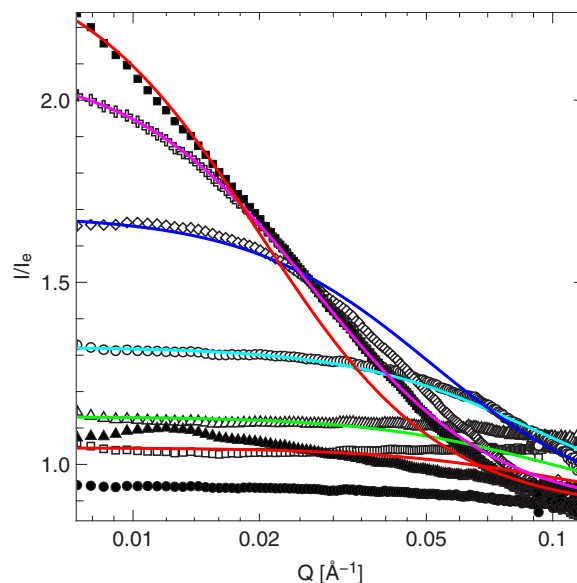
FIG. 4. (Color online) Small-angle scattering as a function of helium filling fraction plotted as the ratio of scattering to scattering from the empty aerogel. Data are for 98% open fraction aerogel. Measurements were made at temperatures between $T = 0.45$ K and $T = 0.60$ K. For clarity not all data are shown. $f_4 = 1\%$ (squares), $f_4 = 2\%$ (triangles), $f_4 = 4\%$ (circles), $f_4 = 8\%$ (diamonds), $f_4 = 12\%$ (crosses), $f_4 = 16\%$ (solid squares), $f_4 = 24\%$ (solid triangles), $f_4 = 100\%$ (solid circles).

limited range, a linear dependence on the filling fraction as shown by the dashed line in Fig. 5(a). The slope of this line is 303 ± 14 Å. This indicates complete filling when the pore size approaches 303 Å.

We propose the following model to explain this linear scaling. Assume the aerogel is composed of a distribution of pores sizes l given by $n(l)$. The volume of a pore of size l is proportional to l^3. In order to explain the linear relation between the total filled volume and the pore size we must have $n(l) \sim l^{-3}$.

Capillary condensation occurs when the crossover length approaches the correlation length of the aerogel as measured
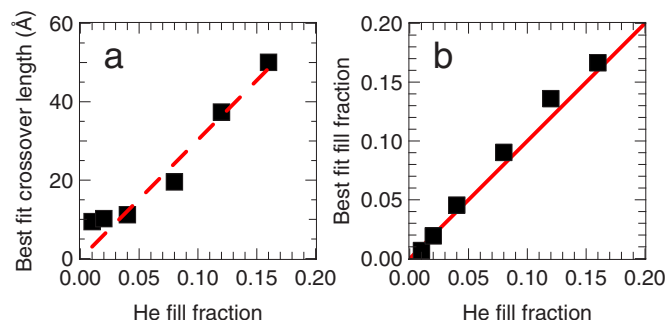
FIG. 5. (Color online) (a) Best-fit values for crossover length and (b) best-fit values for the filling fraction for ^{4}He films in 98% aerogel as a function of nominal filling fraction. The red dashed line in (a) represents the best-fit straight line through the origin with the first three points excluded. The slope is 303 ± 14 Å. The red line in (b) has slope 1, to represent nominal fill fraction equal to the best-fit fill fraction.
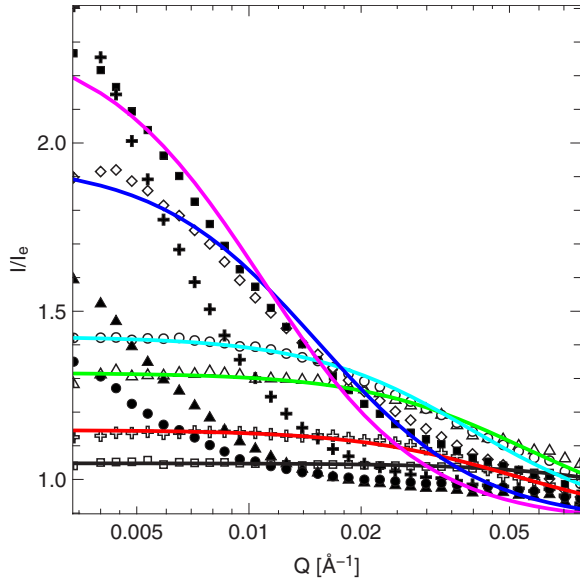
FIG. 6. (Color online) Small-angle scattering as a function of helium filling fraction plotted as the ratio of scattering to scattering from the empty aerogel. Data are for 87% open fraction aerogel. For clarity not all data are shown. Measurements were made at T =0.50 K. f_4=10% (squares), f_4=20% (crosses), f_4=25% (triangles), f_4=30% (circles), f_4=35% (diamonds), f_4=40% (solid squares), f_4=50% (solid crosses), f_4=60% (solid triangles), f_4 =70% (solid circles).

in the fits to the bare aerogel. This suggests that at these length scales there is a capillary condensation event in which the ^{4}He goes from coating strands of the aerogel, to being concentrated in large pores within the aerogel. If intercluster filling is an important aspect of helium-filled aerogel, this argues that theoretical simulations of aerogels [16,18–20] may need to include multiple separately nucleated clusters in order to properly account for the behavior of helium inside the material.

SAXS measurements from a helium-film-filling sequence of 87% open fraction aerogel are shown in Fig. 6, and the resulting fit parameters are then given in Figs. 7(a) and 7(b). As with the 98% aerogel, the model gives a reasonable representation of the data and the x-ray filling fraction is ap-
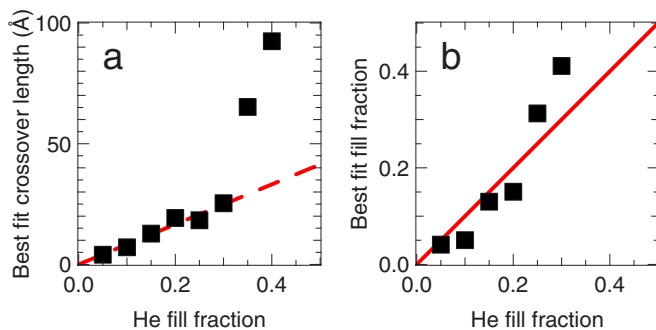
FIG. 7. (Color online) (a) Best-fit values for crossover length and (b) filling fraction for ^{4}He films in 87% aerogel as a function of nominal filling fraction. The dashed line in (a) represents a linear fit through the origin with slope 83±6 Å. The red line in (b) has slope 1, to represent nominal fill fraction equal to the best-fit fill fraction.

proximately equal to the filling fraction obtain by the integrated dosing. A behavior qualitatively similar to the 98% aerogels is observed at the lower filling fraction. The strands become coated with ^{4}He, raising the intensity at small Q and lowering the intensity at large Q. Collapse of the scattering intensity then occurs between 30% and 35% fill fraction. A significant difference shown by this system is that after the intensity collapses, the scattering does not disappear, but rather changes shape to a scattering curve strongly peaked at small Q. The difference between these two systems most likely is due to the higher density of the 87% aerogel, which may result in smaller capillary-condensed regions. It was not possible, however, to go to small enough Q to obtain data that could be used to model the structure of this condensed phase in detail. The crossover lengths L for 87% aerogel are consistently smaller than those obtained from 98% aerogel which is consistent with the higher surface area in the 87% sample. For this system L also scales linearly with the helium dose fraction.

V. HELIUM MIXTURES

A. 98% open volume aerogels

Measurements were next made on aerogels filled with liquid helium mixtures. We first consider liquid helium mixtures in 98% open volume aerogel. The mixtures were dosed into the sample cell at four different fixed volume fractions: X_3=0.40, X_3=0.60, X_3=0.70, and X_3=0.85. A series of SAXS patterns were measured at each volume fraction starting at high temperature and cooling in steps to the base temperature of the cryostat ($\sim$0.45 K). The temperature and volume fractions at which measurements were made are indicated in Fig. 8. The phase diagram in this figure is based on the torsional oscillator measurements of Kim, Ma, and Chan [3].

The measured SAXS patterns at each volume fraction and temperature are shown in Figs. 9–12. The scattering from aerogel filled with helium mixtures shows similarities to the scattering from aerogel with helium films, and we interpret the data in a similar manner. In the present case we modify Eqs. (6) and (7) to describe the contrast upon phase separation between ^{4}He and ^{3}He rather than between ^{4}He liquid and vapor. We assume that the film phase consists of pure ^{4}He giving new expressions for C_1 and C_2:

$$C_1 = [f_{SiO_2}(\rho_{SiO_2} - \rho_{mix}) + f_4(\rho_4 - \rho_{mix})]/f_{SiO_2}\rho_{SiO_2}, \quad (8)$$

$$C_2 = (\rho_{SiO_2} - \rho_4)/\rho_{SiO_2}. \quad (9)$$

Here f_{SiO_2} is the volume fraction occupied by the silica, f_4 is the volume fraction occupied by the pure ^{4}He film, and ρ_{mix} is the electron density of the mixture. Since the total amount of ^{4}He is conserved, the mixture will be depleted in ^{4}He due to the formation of the layer and hence the appropriate value of ρ_{mix} has to be calculated using conservation of ^{3}He. In addition, since the molar volume of the mixtures is not strictly given by a linear interpolation between the molar volumes of the two pure isotopes, we employ the molar volumes measured by Kierstead [21]. The volume fraction re-
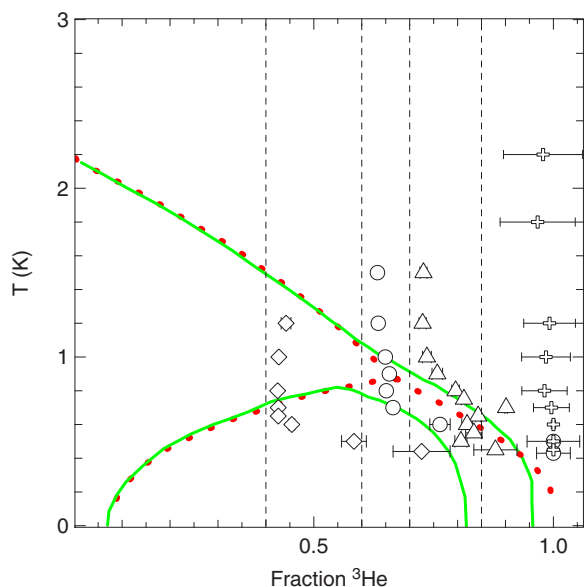
FIG. 8. (Color online) Phase diagram for ^{3}He-^{4}He mixtures in 98% open volume aerogel. Solid green line: measured phase diagram from Kim, Ma, and Chan [3]. Dotted red line: bulk phase diagram. Dashed line: nominal volume fractions for SAXS measurements. Data points: inferred volume fraction left in aerogel after formation of pure ^{4}He film. Diamonds: $\phi=0.40$. Circles: $\phi=0.60$. Triangles: $\phi=0.70$. Crosses: $\phi=0.85$.

maining in the mixture must satisfy the relation

$$(1 - f_{SiO_2})\frac{\phi_0}{\nu_0} = \frac{\phi_{mix}}{\nu_{mix}}(1 - f_4). \tag{10}$$

Here ϕ_0 is the initial molar fraction of ^{3}He and ν_0 the corresponding molar volume. Similarly, ϕ_{mix} and ν_{mix} are the values for the mixture after depletion of ^{4}He. Equation (10) can be solved numerically to yield ϕ_{mix} for any given value of the volume fraction in the film phase, f_4. The fits were furthermore constrained by the condition that the total amount
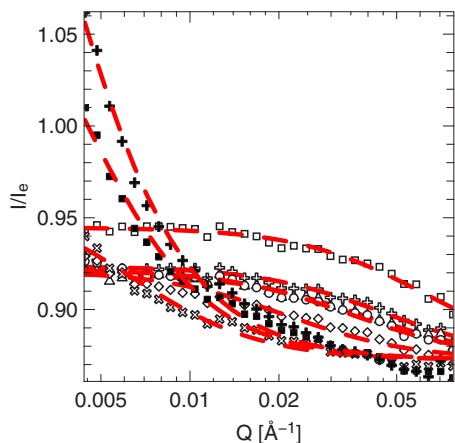
FIG. 9. (Color online) SAXS collected for 98% open volume aerogel at $\phi=0.40$. Squares: $T=1.20$ K. Crosses: $T=1.00$ K. Triangles: $T=0.80$ K. Circles: $T=0.70$ K. Diamonds: $T=0.65$ K. Rotated crosses: $T=0.60$ K. Solid squares: $T=0.50$ K. Solid crosses: $T=0.44$ K. Lines are fits to the model described in the text.
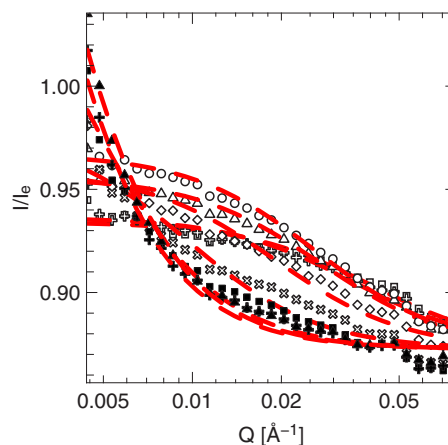
FIG. 10. (Color online) SAXS collected for 98% open volume aerogel at $\phi=0.60$. Squares: $T=1.50$ K. Crosses: $T=1.20$ K. Triangles: $T=1.00$ K. Circles: $T=0.90$ K. Diamonds: $T=0.80$ K. Rotated crosses: $T=0.70$ K. Solid squares: $T=0.60$ K. Solid crosses: $T=0.50$ K. Solid triangles: $T=0.43$ K. Lines are fits to the model described in the text.

of helium in the film phase cannot exceed the amount of ^{4}He initially present.

The normalized SAXS data measured at $X_3=0.40$ are shown in Fig. 9. The solid red lines show the results of the best fit of this model to the data with the parameters L and f_4 varied. In addition, the overall amplitude was varied by $\sim 3\%$ to reflect a small uncertainty in the normalization of the data relative to the empty cell. The values of the fit parameters are plotted in Fig. 13. The depleted value of ϕ_{mix} obtained from Eq. (10) is also plotted as the points in Fig. 8. The data at the three highest temperatures 1.2, 1.0, and 0.8 K are nearly identical and are consistent with the formation of a thin ($\sim$1-nm) film of ^{4}He from the mixture. The data at 0.7 and 0.65 K show a gradual increase in film thickness. The
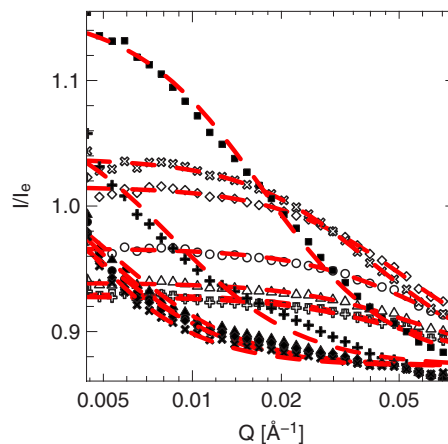
FIG. 11. (Color online) SAXS collected for 98% open volume aerogel at $\phi=0.70$. Squares: $T=1.50$ K. Crosses: $T=1.20$ K. Triangles: $T=1.00$ K. Circles: $T=0.90$ K. Diamonds: $T=0.80$ K. Rotated crosses: $T=0.75$ K. Solid squares: $T=0.70$ K, Solid crosses: $T=0.65$ K. Solid triangles: $T=0.60$ K. Solid circles: $T=0.55$ K. Solid diamonds: $T=0.50$ K. Solid rotated crosses: $T=0.45$. Lines are fits to the model described in the text.
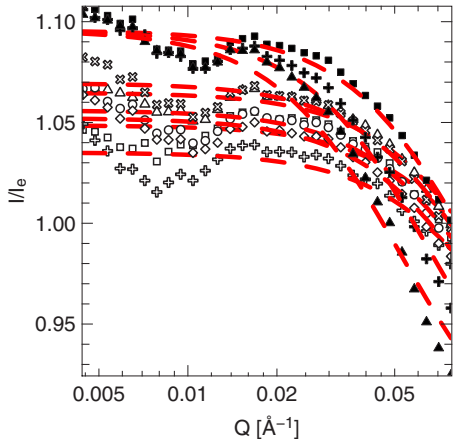
FIG. 12. (Color online) SAXS collected for 98% open volume aerogel at $\phi=0.85$. Squares: $T=2.20$ K. Crosses: $T=1.80$ K. Triangles: $T=1.20$ K. Circles: $T=1.00$ K. Diamonds: $T=0.80$ K. Rotated crosses: $T=0.70$ K. Solid squares: $T=0.60$ K. Solid crosses: $T=0.50$ K. Solid triangles: $T=0.45$ K. Lines are fits to the model described in the text.

film rapidly thickens below 0.65 K, a temperature which also corresponds closely to the temperature of phase separation for the bulk phase diagram.

Fits to the data at $X_3=0.60$ (Fig. 10) show similar results. The film thickness remains fairly constant at temperatures above the bulk ^{3}He-^{4}He phase-separation point and then rapidly increases upon crossing the bulk phase line. A different behavior is seen, however, for the 70% volume fraction data. Upon reaching the phase separation line the film thickens, but instead of entering the two-phase region, the removal of ^{4}He from the mixture pushes the mixture back onto the phase coexistence line. The mixture volume fraction then appears to track, albeit with a large uncertainty, the phase coexistence line down to the lowest temperature measured.

For the data at $X_3=0.85$ the initial film phase is slightly thinner than for the phases at lower X_3. The helium film thickness begins to increase at temperatures just above the bulk phase separation point. Eventually, the film grows until all of the ^{4}He segregates to the film phase, leaving $\phi_{mix}=1$. The data at 85% volume fraction also show a slight dip around $Q=0.01$ Å^{-1}. This is probably not a real effect but
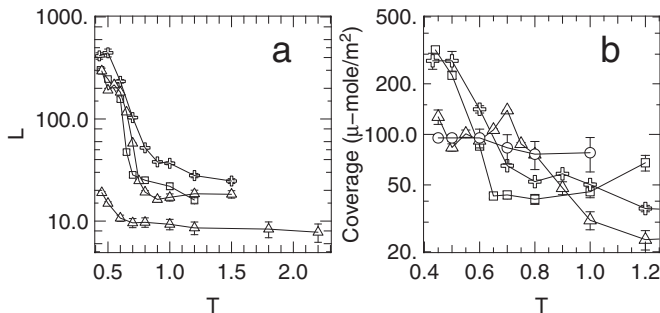
FIG. 13. (a) Best-fit values of crossover length for 98% open fraction aerogel as a function of ^{3}He volume fraction and (b) for the helium coverage. Squares: $\phi=0.40$. Crosses: $\phi=0.60$. Triangles: $\phi=0.70$. Circles: $\phi=0.85$. The lines are guides to the eye.
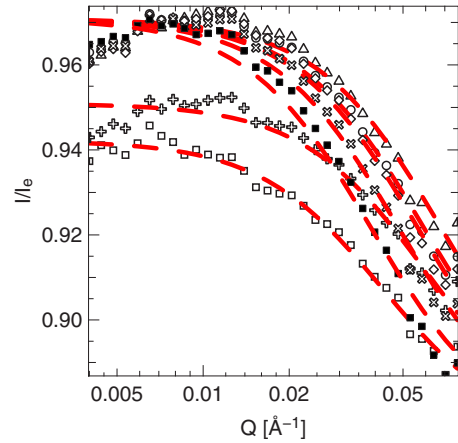
FIG. 14. (Color online) SAXS collected for 87% open volume aerogel at $\phi=0.34$. Squares: $T=1.80$ K. Crosses: $T=1.50$ K. Triangles: $T=1.20$ K. Circles: $T=1.00$ K. Diamonds: $T=0.90$ K. Rotated crosses: $T=0.80$ K. Solid square: $T=0.70$ K. Solid crosses: 0.60 K. Solid triangles: 0.50 K. Lines are fits to the model described in the text.

resulted from a small change in the alignment of the x-ray beam during that portion of the measurement relative to the time when the reference empty cell was measured.

It is interesting to plot the amount of helium observed in the film phase in units of μmol/m^2 in order to make contact with previous adsorption measurements. The 98% open volume aerogel has a surface area of $A_0 \approx 1000$ m^2/g. Thus the effective coverage is given by $\sigma=f_4/(\rho_{SiO2}f_{SiO2}A_0\nu_4)$, where ν_4 is the molar volume of ^{4}He. (Since ν_4 is used to calculate ρ_4 and then f_4 in the fits, this cancels out in the calculation.) These values are displayed in Fig. 13. For the $X_3=0.40$ data at high temperature, the value of σ comes out to around 30 μmol/m^2. In the work of Paetkau and Beamish [11] it was found that superfluidity would not begin for adsorption of pure ^{4}Hefilms until a coverage of 30.7 μm/m^2 was deposited. They called the initial nonsuperfluid helium coverage the "dead layer." It is interesting that this dead layer value is very close to the value found by us for the coverage as determined by SAXS at the same temperature. However, Paetkau and Beamish found that for helium mixtures, the dead layer value changed to a ^{4}He coverage of 37 μmol/m^2.

B. 87% open volume aerogels

The results of scattering from mixtures in 87% open volume aerogel are shown in Figs. 14–16. The data were fit to same model as described earlier. Figure 17 shows the volume fraction of ^{3}He remaining in the mixture after depletion due to the formation of a film. Figure 18 shows the variation of the crossover length L and the inferred film coverage at the three measured volume fractions of 0.34, 0.50, and 0.60. The model provides a good description of the data, although fit parameters show some variability, especially at $X_3=0.34$. The fit results for the film thickness in 87% aerogels are, however, qualitatively different than those for the 98% aerogel. No transition occurs from a film state to a pore filling state. Rather, the film gradually thickens until it exhausts the
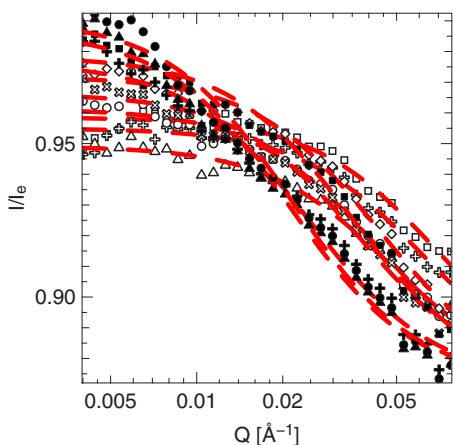
FIG. 15. (Color online) SAXS collected for 87% open volume aerogel at $\phi=0.50$. Squares: $T=1.80$ K. Crosses: $T=1.50$ K. Triangles: $T=1.00$ K. Circles: $T=0.90$ K. Diamonds: $T=0.80$ K. Rotated crosses: $T=0.70$ K. Solid squares: $T=0.60$ K. Solid crosses: 0.50 K. Solid triangles: 0.46. Lines are fits to the model described in the text.

available ^{4}He. The inferred coverage for the helium in 87% aerogel is quite similar to that found for 98% aerogel.

VI. DISCUSSION

The most significant open question left by previous studies of helium mixtures in aerogel is the nature of the ^{3}He-rich superfluid phase. Does superfluidity exist within the mixture itself or only within a helium film? The SAXS results clearly show that a film phase forms on the aerogel and furthermore that this film thickens across the phase boundary. These results back up the model suggested by Mulders and Chan [9], as well as by Tulimieri, Yoon, and Chan [12], that superfluidity occurs in a thickened film phase and that, since this film is thick, there is a bulklike character to the phase transition. However, while these previous measurements only inferred
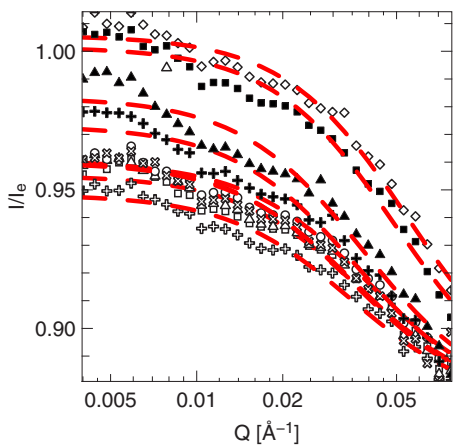
FIG. 16. (Color online) SAXS collected for 87% open volume aerogel at $\phi=0.60$. Squares: $T=1.80$ K. Crosses: $T=1.20$ K. Triangles: $T=0.90$ K. Circles: $T=0.80$ K. Diamonds: $T=0.70$ K. Rotated crosses: $T=0.60$ K. Solid squares: $T=0.45$ K. Lines are fits to the model described in the text.
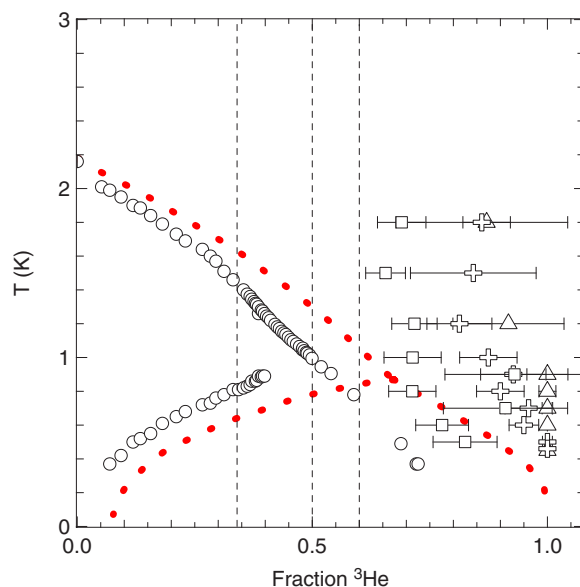
FIG. 17. (Color online) Phase diagram for ^{3}He-^{4}He mixtures in 87% open volume aerogel. Circles: measured phase diagram from Paetkau and Beamish [11]. Dotted red line: bulk phase diagram. Dashed line: nominal volume fractions for SAXS measurements. Data points: inferred volume fraction left in aerogel after formation of pure ^{4}He film. Squares: $\phi=0.34$. Crosses: $\phi=0.50$. Triangles: $\phi=0.60$.

that the width of the film thickened, in the present work we explicitly measure the crossover length between the film and mixed phase as shown in Figs. 13(a) and 18(a).

A thickening film phase also explains the shift of the phase diagram in aerogel, relative to the phase diagram in bulk, and the separation of the λ line from the phase separation line. The phase diagram in aerogels is shifted, due to the change in the concentration of the mixture after depletion of ^{4}He into the film. The λ line separates because the superfluid transition occurs in a thick-film state which does not require complete phase separation. This is seen specifically for the data sets in 98% aerogel. At $X_3=0.60$ and $X_3=0.70$ the film begins to thicken slightly before the bulk separation temperature. Once the film has thickened enough it becomes superfluid, leading to the observed λ line. It is only at lower temperatures that the film thickness diverges, leading to a
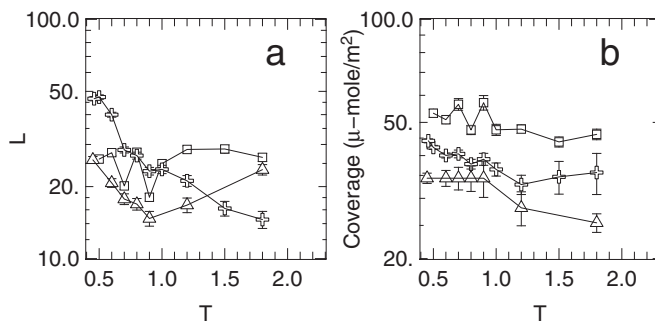
FIG. 18. (a) Best-fit values of crossover length for 87% open fraction aerogel as a function of ^{3}He volume fraction and (b) for the helium coverage. Squares: $\phi=0.34$. Crosses: $\phi=0.50$. Triangles: $\phi=0.60$.

signature of a phase separation. Thus the ^{3}He-rich superfluid phase corresponds to volume fractions where there is enough helium to thicken the film to the point where it becomes superfluid, but not yet enough to instigate phase separation, which only occurs when further helium is expelled from the mixture as the temperature is lowered. For higher volume fractions—e.g., $X_3 = 0.85$—the mixture is completely depleted of ^{4}He and the film never thickens enough to show phase separation. This argument also explains why superfluidity is not seen at all above $X_3 = 0.96$ since at this volume fraction, even if all the ^{4}He segregates to the film phase, it can only form a coverage of 25 μmol/m^2 which is very close to the threshold of 27.85 μmol/m^2 found by Agnolet, McQueeney, and Reppy to be required for the onset of superfluidity in films [22]. The idea of superfluidity in the film was argued against by Kim, Ma, and Chan, since the superfluid transition in ^{3}He-rich mixtures was qualitatively different from that of pure ^{4}He films. However, their analogy may not be appropriate, because of the significantly lower surface tension between the mixture and the film, as compared to the liquid and the vapor. A smaller surface tension would allow the film to thicken significantly more than in the case of pure films, before the onset of capillary condensation.

The SAXS data also provide a satisfactory explanation of why there is no indication of phase separation at high ^{3}He concentration in 87% open volume aerogels. In this case, there is a much larger surface area per volume of aerogel. Thus, the mixture is depleted of ^{4}He more quickly than in the case for 98% open volume aerogels. For values of $X_3 < 0.80$ the film can thicken enough to become superfluid, but not enough to commence capillary condensation. For higher values of X_3 the film thickness remains too small to obtain superfluidity. This is also consistent with the results of Tulimieri, Yoon, and Chan [12] who found a phase diagram in porous gold that was similar to the phase diagram found in 98% aerogel. Since the surface area per unit volume of the porous gold ($\sim 1.3 \times 10^5$ m^{-1}) is significantly smaller than of either 87% aerogel ($\sim 2.8 \times 10^6$ m^{-1}) or 98% aerogel ($\sim 4.4 \times 10^5$ m^{-1}), porous gold would not have been able to deplete the mixture of ^{4}He before entering the phase separation region.

The present analysis of SAXS was limited by the assumption that the ^{4}He film phase contains no ^{3}He, and furthermore the effects of the interfacial width were not considered. Neither of these assumptions should be strictly true. However, the addition of parameters to the model profile to allow for a mixed film phase and a finite width interface would prevent the fitting routine from converging on a unique set of parameters. Indeed, it does not seem likely that SAXS data would ever be able to resolve such detailed information about the film phase. It might be possible, however, in future experiments to measure the ^{3}He-^{4}He interface of an oriented film using specular reflectivity. Such a measurement could yield much more detailed information about the profile as has been done previously for the ^{4}He liquid-vapor interface [23].

In conclusion, we have studied the properties of helium mixtures in 98% and 87% open volume aerogels using SAXS. Modeling of the data indicates that a thin ($\sim$1-nm) ^{4}He film is present at all temperatures and that this film begins to thicken at temperatures close the bulk phase-separation line. Based on these results it appears that the ^{3}He-rich superfluid phase has superfluidity within the film, which appears bulklike because the film is thick. Superfluidity no longer exists at high ^{3}He concentrations because all of the ^{4}He has been exhausted and the film cannot grow thick enough. The presence of a superfluid transition in the 87% open volume aerogels can then be explained due to the film thickening, but because of the extra surface area, there is not enough ^{4}He to have the film phase condense into a capillary condensed phase.

[1] M. Chan, N. Mulders, and J. Reppy, Phys. Today **49**(8), 30 (1996).

[2] B. J. Frisken, A. J. Liu, and D. S. Cannell, MRS Bull. **19**(5), 19 (1994).

[3] S. B. Kim, J. Ma, and M. H. W. Chan, Phys. Rev. Lett. **71**, 2268 (1993).

[4] A. Falicov and A. N. Berker, Phys. Rev. Lett. **74**, 426 (1995).

[5] A. N. Berker, J. Appl. Phys. **70**, 5941 (1991).

[6] A. N. Berker, Physica A **194**, 72 (1993).

[7] M. Blume, V. J. Emery, and R. B. Griffiths, Phys. Rev. A **4**, 1071 (1971).

[8] A. Maritan, M. Cieplak, M. R. Swift, F. Toigo, and J. R. Banavar, Phys. Rev. Lett. **69**, 221 (1992).

[9] N. Mulders and M. H. W. Chan, Phys. Rev. Lett. **75**, 3705 (1995).

[10] P. A. Crowell, J. D. Reppy, S. Mukherjee, J. Ma, M. H. W. Chan, and D. W. Schaefer, Phys. Rev. B **51**, 12721 (1995).

[11] M. Paetkau and J. R. Beamish, Phys. Rev. Lett. **80**, 5591 (1998).

[12] D. J. Tulimieri, J. Yoon, and M. H. W. Chan, Phys. Rev. Lett. **82**, 121 (1999).

[13] T. Freltoft, J. K. Kjems, and S. K. Sinha, Phys. Rev. B **33**, 269 (1986).

[14] D. Posselt, J. S. Pederson, and K. Mortensen, J. Non-Cryst. Solids **145**, 128 (1992).

[15] J. Teixeira, in *On Growth and Form*, edited by H. Stanley and N. Ostrowsky (Nijhoft, Dordrecht, 1988), p. 145.

[16] A. Hasmy, E. Anglaret, M. Foret, J. Pelous, and R. Jullien,

Phys. Rev. B **50**, 6006 (1994).

[17] B. J. Frisken, D. S. Cannell, M. Y. Lin, and S. K. Sinha, Phys. Rev. E **51**, 5866 (1995).

[18] R. Salazar, R. Toral, and A. Chakrabarti, J. Sol-Gel Sci. Technol. **15**, 175 (1999).

[19] J. V. Porto and J. M. Parpia, Phys. Rev. B **59**, 14583 (1999).

[20] F. Detcheverry, E. Kierlik, M. L. Rosinberg, and G. Tarjus, Phys. Rev. E **68**, 061504 (2003).

[21] H. Kierstead, J. Low Temp. Phys. **24**, 497 (1976).

[22] G. Agnolet, D. F. McQueeney, and J. D. Reppy, Phys. Rev. B **39**, 8934 (1989).

[23] L. B. Lurio, T. A. Rabedeau, P. S. Pershan, I. F. Silvera, M. Deutsch, S. D. Kosowsky, and B. M. Ocko, Phys. Rev. Lett. **68**, 2628 (1992).